Transfer and surface vibration couplings in the fusion of $^{40}Ca+^{46,48,50}Ti$ at near-barrier energies

A. A. Sonzogni, J. D. Bierman,* M. P. Kelly, J. P. Lestone, J. F. Liang,† and R. Vandenbosch
Nuclear Physics Laboratory, Box 354290, University of Washington, Seattle, Washington 98195
(Received 11 July 1997)

Fusion and quasielastic excitation functions were measured for $^{40}Ca+^{46,48,50}Ti$ at energies close to the Coulomb barrier. The interest in these systems lies in the opposite target-mass dependence of surface vibration couplings and neutron-transfer couplings. The cross sections were measured at small energy steps and with high precision, so that the structure in the excitation functions (barrier distributions) could be revealed through a differentiation process. The subbarrier fusion data show a larger enhancement with increasing target mass number, which clearly indicates the importance of transfer couplings. The agreement between the fusion and quasielastic barrier distributions is quite good. Simplified coupled-channel calculations were performed to reproduce the fusion data. A very good agreement is obtained by coupling to low lying excited states (2^+ and 3^-) and to the most positive neutron-transfer Q value (two-neutron projectile pickup channel). [S0556-2813(98)01402-2]

PACS number(s): 25.70.Jj, 25.70.Bc, 24.10.Eq

I. INTRODUCTION

One interesting aspect of nuclear reactions involving heavy ions at energies close to the Coulomb barrier is the coupling of the internal degrees of freedom to the relative motion of the colliding nuclei. This coupling influences the quantum tunneling that leads to fusion, and can induce large enhancements of the fusion cross section at bombarding energies below the energy of the one-dimensional barrier representing only the relative motion of inert nuclei [1]. Three factors have been identified as playing a major role in the magnitude of the subbarrier fusion cross sections: permanent nuclear deformation, coupling to low lying nuclear excited states, and neutron-transfer reactions. The occurrence of the first two seems to be firmly accepted based on very compelling experimental evidence [2–4], while the role of neutron-transfer reactions is less clear.

The influence of nuclear deformation is straightforward. For instance, if the target nucleus is prolate, the Coulomb field at its tips is lower than in the equatorial area, which will then increase the fusion probability at subbarrier energies. Spherical nuclei can become deformed by surface vibrations, leading to an increase in the near-barrier fusion cross section due to the excitation of low lying nuclear states. The importance of neutron transfer on nuclear fusion originates from the fact that neutrons are insensitive to the Coulomb field; therefore they can start being transferred at larger separations than other particles. A correlation between the overall transfer strength and fusion enhancement was noticed early by Henning *et al.* [5]. One possible scenario is that before fusion takes place, a flow of neutrons between target and projectile has already started [6]. In consequence, it is thought that if a system exhibits neutron-transfer reactions (either stripping or pickup) with positive Q values, then the subbarrier fusion cross sections will increase [6,7].

Typically one tries to deduce the important parameters in characterizing near-barrier fusion dynamics by measuring and comparing the fusion excitation function for different systems. Projectiles and targets are chosen to highlight the specific characteristic which is under study. For instance, one of the pioneering works to study the effect of nuclear deformation focused on $^{16}O+^{144,154}Sm$ [8,9]. Both the projectile and ^{144}Sm are spherical, but nuclear deformation increases as the Sm isotopes become heavier. In a similar fashion, several experiments were performed to understand the effect of transfer reactions [6,7,10]. As before, the choice of the projectile-target combination is crucial, and for the systems studied it is often difficult to make unambiguous statements regarding transfer reactions when the system also contains a strong coupling to surface vibrations. Transfer Q values become more positive as the surface vibration couplings increase in all these systems and there is not enough information to understand the subtle interplay of surface vibration and transfer couplings.

It would thus be interesting to study a system where the opposite happens, i.e., where collectivity decreases when the transfer probability increases. In the present work the projectile was chosen to be a double-magic and neutron-deficient nucleus. The criteria used to select the targets were that they should be a series of even-even isotopes, with the heaviest isotope closest to a neutron closed shell. In this way, the heavier the target, the less negative (or more positive) the neutron-transfer Q values, and because of the closeness to a closed shell, the smaller the phonon-coupling-induced enhancement. Among the very few candidates that match these requirements, the systems $^{40}Ca+^{46,48,50}Ti$ were chosen for the present study.

In the last few years we have witnessed a considerable rise in the precision and amount of subbarrier fusion cross section data taken for a particular system under study. This is mainly because the goal of most current fusion experiments is to reveal the structure of the fusion excitation function due to the coupling to internal degrees of freedom. For instance, if both target and projectile are spherical, there is a single

*Permanent address: Physics Department AD-51, Gonzaga University, Spokane, WA 99258-0051.
†Permanent address: Physics Division, Oak Ridge National Laboratory, Oak Ridge, TN 37831.

Coulomb barrier, but if the target is deformed, there is a distribution of barriers, with each one corresponding to a given orientation angle of the target with respect to the beam axis [2]. Similarly, it has been found that the effect of surface vibration excitation and neutron-transfer reactions is to replace the single barrier with a distribution of barriers [4,7]. Knowledge of the fusion barrier distribution can help greatly in the interpretation of the data because it more clearly points out the mechanisms that govern the near-barrier fusion. However, the extraction of barrier distributions from the fusion excitation function is a considerable experimental challenge which demands great precision in the measurements.

Because of the interest that barrier distributions possess, other ways of extracting them have been explored [11,12]. Briefly, by arguing that fusion information is also present in the quasielastic and elastic differential cross sections at angles close to the grazing angle, methods to obtain barrier distributions from quasielastic and elastic excitation functions at a fixed angle have been proposed. One of the reasons why these ideas are interesting is the fact that experiments designed to measure elastic and quasielastic excitation functions are easier to perform than fusion ones. It was decided that these suggestions were important enough to be investigated.

In summary, it was considered that knowledge of the fusion excitation functions at near-barrier energies for ^{40}Ca $+^{46,48,50}$Ti would be of help in understanding the effect of surface vibration couplings (SVC's) and neutron-transfer couplings (TC's) in the nuclear fusion dynamics. Our data were measured with high enough precision so that barrier distributions could be extracted. In addition, an experiment to measure the elastic-quasielastic excitation function was performed in order to obtain the elastic-quasielastic barrier distributions.

II. EXPERIMENTS

The experiments were performed using 97–150 MeV ^{40}Ca beams from the University of Washington's Tandem-Linac accelerator facility. The rf of the Linac was used for precise timing measurements. The Ti targets were self-supported, had areal densities of around 200 μgm/cm^2, and isotopic purities of 90%, 99%, and 90% for ^{46}Ti, ^{48}Ti, and ^{50}Ti, respectively.

A. Fusion experiments

At the bombarding energies of interest, fusion of ^{40}Ca with the Ti targets leads to heavy evaporation residues (ER's), which were detected with a set of two Si detectors mounted in tandem. The thickness of the first element (ΔE) was adjusted to optimize the distinction between ER's and scattered beamlike particles. The ΔE thickness was around 8 μm and ER's could punch through it. The second detector was used to veto out projectilelike events. The identification of ER's was performed with the help of energy and time-of-flight information. A typical plot of the energy deposited in the ΔE detector vs time of flight can be seen in Fig. 1. Two Si detectors were placed symmetrically at $\pm 27°$ with respect to the beam line for normalization purposes.

The total fusion cross sections were obtained from the differential cross sections in a way similar to the one described in Ref. [13]. Briefly, angular distributions are measured at a selected number of energies. Then a function (usually a double Gaussian) is fitted to match the data and then integrated to obtain the total fusion cross section. The ratio between the differential cross section at a given angle to the total cross section is obtained as a function of the beam energy. Finally, only differential cross sections are measured for the remaining energies, which are thereafter converted to a total cross section.

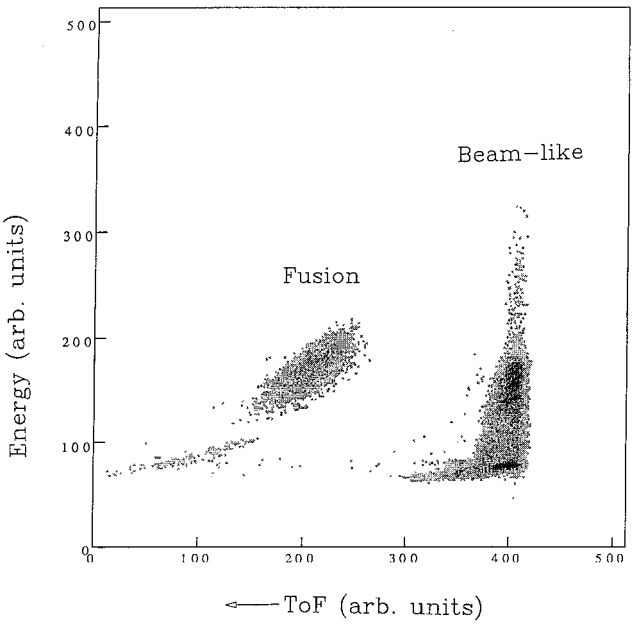

FIG. 1. Energy versus time-of-flight (ToF) plot for ^{40}Ca+^{50}Ti at $\theta=5°$ and $E_{\rm lab}=118$ MeV. Fusion and beamlike events are indicated.

Evaporation residue angular distributions were measured for angles larger than 4° with respect to the beam direction, at ^{40}Ca laboratory energies of 110, 120, 130, and 150 MeV. The total cross section was obtained after fitting and integrating a double Gaussian. For example, the ER angular distributions for ^{40}Ca+^{46}Ti are shown in Fig. 2. For a larger set of energy, only differential cross sections were measured at 5°, and from them, the total ER cross sections were obtained. The resulting fusion excitation functions are plotted in Fig. 3, where the points are plotted at an energy which corresponds to the energy at the middle of the target.

B. Elastic-quasielastic experiment

Experiments performed to measure the elastic differential cross section at large angles are not easy for systems with a high degree of mass symmetry [14,15]. To understand the reason, it has to be remembered that for symmetric systems the projectile can transfer a large amount of kinetic energy to the target, and therefore near-grazing-angle events have quite small values of energies. As an example, Fig. 4 shows the energy of both the elastically scattered projectile and the target recoil as a function of the laboratory detection angle for ^{40}Ca at 114 MeV. When this kinematical effect is combined with the finite value of the target thickness, the events to be detected have an energy distribution with a low mean value and a large dispersion.

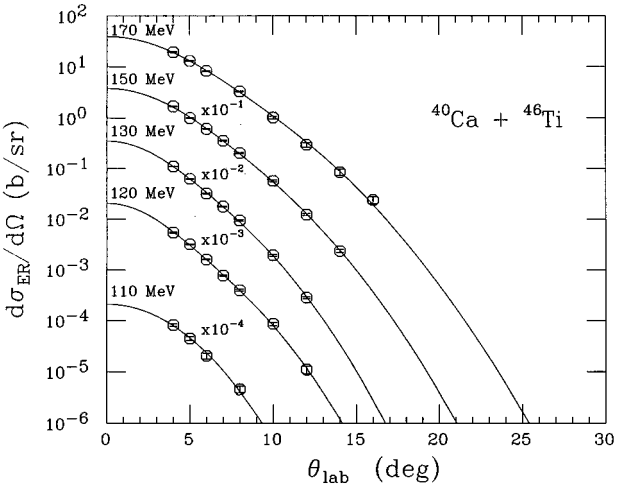

FIG. 2. Angular distributions of evaporation residues for the ^{40}Ca+^{46}Ti system. The solid curves are the fits used to obtain the angle-integrated cross sections.

The experimental setup consisted of two 100-μm-thick movable Si detectors placed at angles close to the grazing angle, plus a Si monitor fixed at 15.5°. All the detectors gave both energy and time-of-flight information, which was very useful in distinguishing between elastically scattered projectiles and target recoils. A typical two-dimensional plot of energy versus time of flight is shown in Fig. 5.

Data were taken at four different laboratory angles 56°, 65°, 66°, and 75°. Since we were interested in scattering events at near grazing angles, only the projectile events in Fig. 5 were used to deduce fusion information. As an example, the resulting projectile excitation functions for ^{40}Ca +^{48}Ti can be seen in Fig. 6.

III. INTERPRETATION OF THE RESULTS

A. Comparison of the fusion excitation functions

When the fusion excitation function is measured for a number of systems, a useful and model-independent comparison between them can be made by using the expression [1]

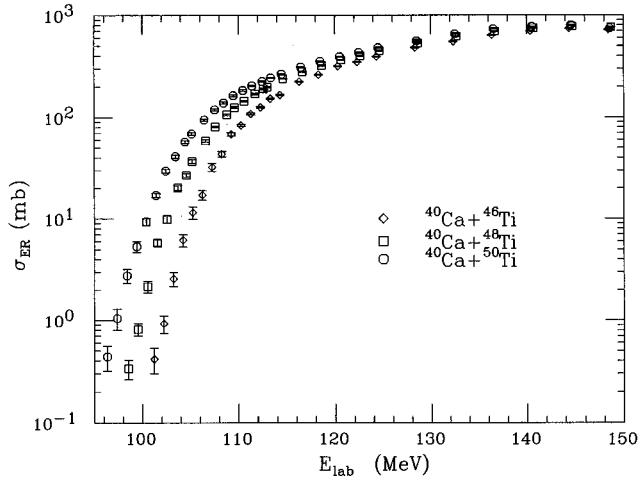

FIG. 3. ER excitation functions for ^{40}Ca+^{46,48,50}Ti.

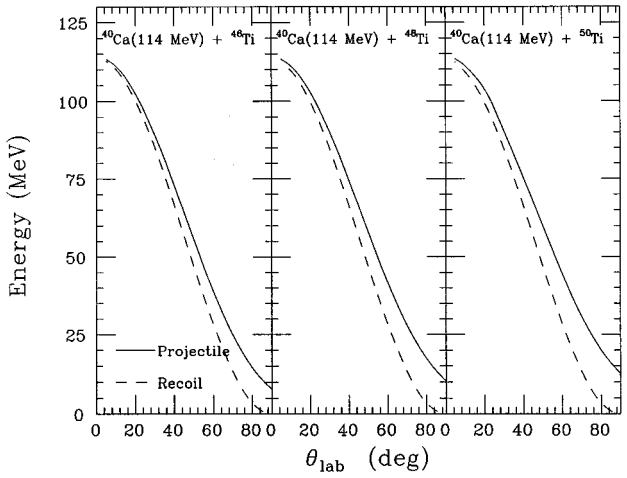

FIG. 4. Kinetic energy of elastically scattered projectile and recoil as a function of $\theta_{\rm lab}$ for ^{40}Ca+^{46,48,50}Ti.

$$\sigma_{\rm fus}(E)=\pi R_{\rm fus}^2(1-V_b/E), \tag{1}$$

which is valid for energies (a) larger than the Coulomb barrier (V_b) and (b) small enough so that preequilibrium and/or friction processes are not taking place. This equation can be rearranged to give

$$E\sigma_{\rm fus}(E)=\pi R_{\rm fus}^2(E-V_b), \tag{2}$$

from which it can be seen that a linear fit of the product $E\sigma_{\rm fus}(E)$ in the region where quantum tunneling or preequilibrium/friction effects are not important should produce values of $R_{\rm fus}$ and V_b. Once obtained, they can be used to correct the corresponding excitation functions for differences in barrier heights and fusion radii.

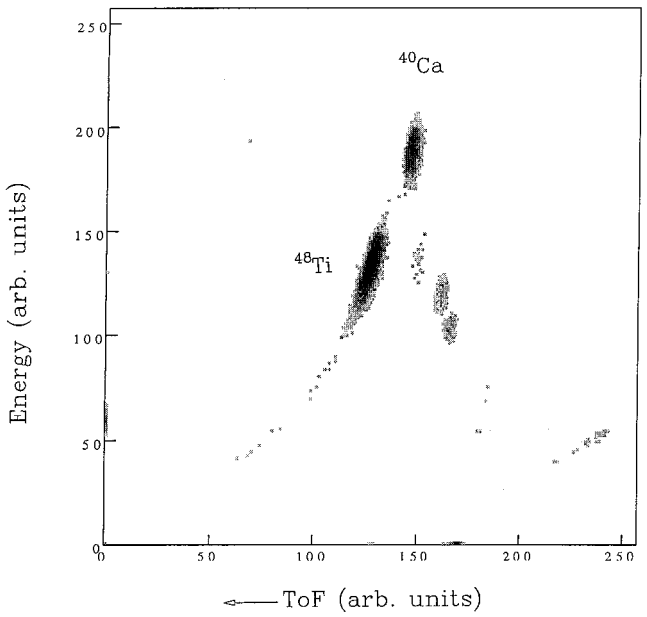

FIG. 5. Energy versus time-of-flight spectra at $\theta=56°$ for 107 MeV ^{40}Ca+^{48}Ti. Elastically scattered projectiles and recoils are indicated.

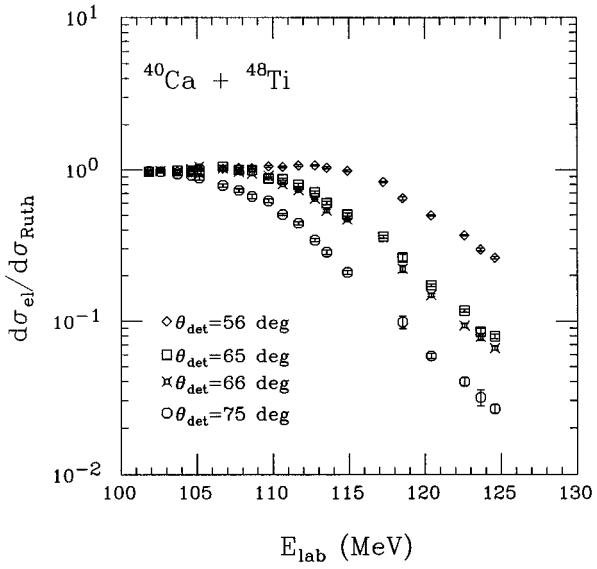

FIG. 6. Elastic scattering excitation functions normalized to Rutherford scattering cross section at four different detection angles for ^{40}Ca+^{48}Ti.

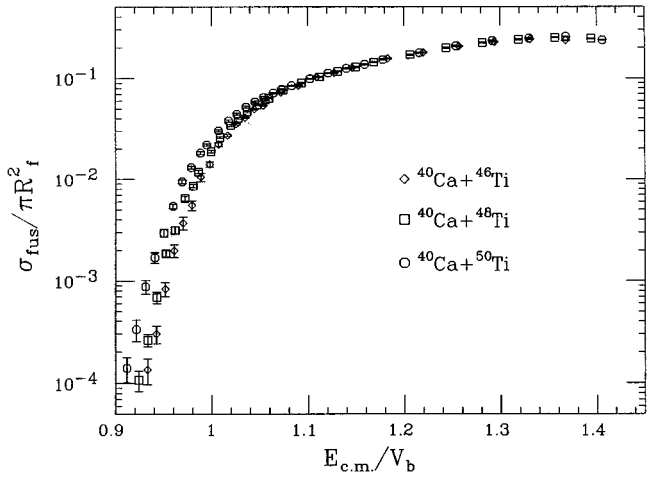

FIG. 7. Reduced fusion cross section as a function of the ratio of the center-of-mass energy to the height of the fusion barrier V_b for ^{40}Ca+^{46,48,50}Ti.

In the present case, the results of the fit procedure are listed in Table I, while the values of $\sigma_{fus}/\pi R^2_{fus}$ are plotted in Fig. 7 as a function of E/V_b. In this way, the high energy part of the data is scaled to be the same, with the purpose of revealing differences in the quantum tunneling. The most striking feature in this figure is the magnitude of the reduced cross section at subbarrier energies, particularly the target-mass dependance. As it was mentioned in the introduction, if SVC's dominate over TC's, the subbarrier reduced cross sections for ^{40}Ca+^{50}Ti cannot be larger than those for ^{40}Ca +^{46}Ti. Thus, we have demonstrated in a model-independent way that TC's dominate over SVC's in the ^{40}Ca+^{50}Ti system.

Similar results for the role of the neutron-transfer Q value on subbarrier fusion enhancement have also been found for ^{40}Ca+^{40,48}Ca [16] and ^{40}Ca+^{90,96}Zr [10]. The design of these experiments was similar to ours, taking a neutron-deficient projectile and two targets, one of which is neutron poor while the other is neutron rich. The Zr measurements are of special interest because of the high precision and quality of the data. In addition, the differences in neutron-transfer Q values between the two Zr isotopes is much larger than between the Ti ones, which in turn makes the influence of the neutron transfer far more evident. On the other hand, the lighter of the Zr isotopes has a neutron closed shell, and therefore some of the subbarrier enhancement for ^{40}Ca +^{96}Zr can be due to SVC's rather than to TC's.

TABLE I. Fusion radius and Coulomb barrier values extracted from the fusion excitation functions.

System	R_f (fm)	$V_b^{c.m.}$ (MeV)
^{40}Ca+^{46}Ti	9.92±0.08	58.03±0.73
^{40}Ca+^{48}Ti	9.97±0.07	58.17±0.62
^{40}Ca+^{50}Ti	10.05±0.07	58.71±0.61

B. Fusion barrier distributions

The fusion barrier distribution is defined as [17]

$$D_{fus}(E) = d^2[E\sigma_{fus}(E)]/dE^2. \quad (3)$$

Since a second derivative of a rather smooth function is involved, high precision in the determination of the fusion cross section and the energy of the beam is required. In the present case, systematic uncertainties in the cross sections may be present since the ER detector did not take data for angles smaller than 4°. Although this systematic error may change slightly the magnitude of the barrier distribution, it will not change its shape. On the positive side, the relative efficiency of the detectors was precisely determined by using an alpha source.

Two different methods were used to extract the fusion barrier distributions. One of them involves the use of the so-called ''point difference procedure'' [13], which has been extensively used. The other obtains the derivatives through a straight line fit to each set of three adjacent points. The slope obtained from the fit was assumed to be a good estimate of the first derivative around the middle point. In both cases, the center-of-mass energy interval between the points was about 1.1 MeV and barrier distributions were extracted for $E_{c.m.} < 67$ MeV. The two methods agreed well as can be seen in Fig. 8.

As was mentioned at the beginning of this section, barrier distributions require very precise measurements. Regarding the results from the present experiment, whose emphasis was on comparison of cross sections for different systems rather than on extracting detailed information from barrier distributions, one should look for trends rather than for details. From Fig. 8 it is clear that as one moves from ^{46}Ti to ^{50}Ti, $D_{fus}(E)$ becomes shorter and broader. This trend will be compared with expectations from coupled-channel calculations in a later section.

C. Elastic-quasielastic barrier distributions

As mentioned in the Introduction, it has been suggested that barrier distributions can be obtained from both elastic

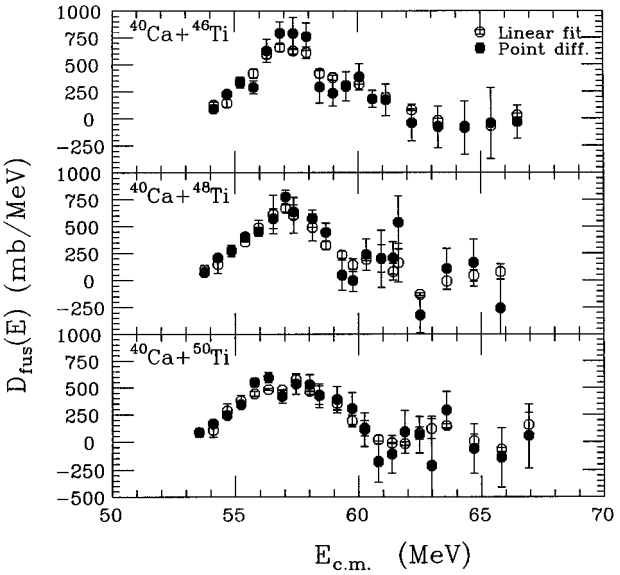

FIG. 8. Fusion barrier distributions for ^{40}Ca+^{46,48,50}Ti as a function of the center-of-mass energy.

and quasielastic data. Briefly, if the experimental information consists of a quasielastic scattering excitation function, the equation

$$D_{\mathrm{qel}}(E) = -\frac{d}{dE}\left(\frac{d\sigma_{\mathrm{qel}}}{d\sigma_R}\right) \tag{4}$$

is used to obtain $D_{\mathrm{qel}}(E)$ [11]. Here the ratio $d\sigma_{\mathrm{qel}}/d\sigma_R$ corresponds to

$$\frac{d\sigma_{\mathrm{qel}}}{d\Omega} \Big/ \frac{d\sigma_{\mathrm{Rutherford}}}{d\Omega}.$$

For elastic scattering, $D_{\mathrm{el}}(E)$ is given by [12]

$$D_{\mathrm{el}}(E) = -\frac{d}{dE}\left(\frac{d\sigma_{\mathrm{el}}}{d\sigma_R}\right)^{1/2}. \tag{5}$$

The relation between these barrier distributions and that for fusion is taken [11,12] as

$$D_{\mathrm{fus}}(E) = \pi R_{\mathrm{fus}}^2 D_{\mathrm{qel,el}}(E). \tag{6}$$

The present experiment could not distinguish between elastic and quasielastic events. It has been explained that because of the high degree of mass symmetry for the systems under study, the elastic peak has a broad energy distribution at large scattering angles, which causes it to overlap with inelastic and transfer events. Therefore, the data obtained should be considered quasielastic rather than elastic. However, for comparison purposes, barrier distributions were also extracted assuming that the data are purely elastic or that they have inelastic contributions. To obtain the first derivatives, a straight line fit was performed to each set of three adjacent points. The slope obtained from the fit was assumed to be a good estimate of the first derivative around the middle point. The laboratory energy interval between the points was about 1 MeV for energies lower than 116 MeV and 2 MeV for larger energies.

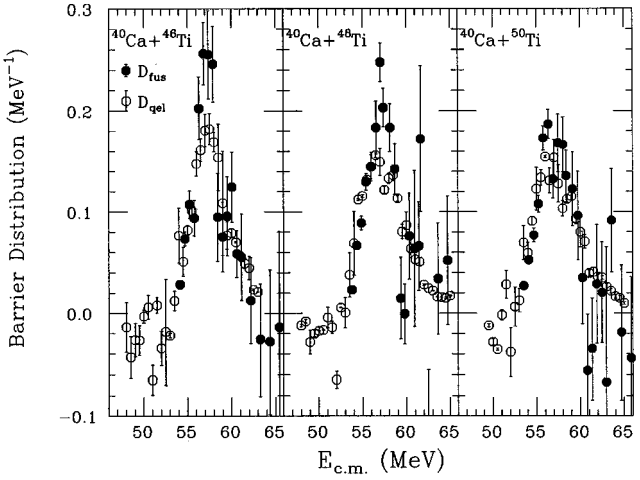

FIG. 9. Comparison between quasielastic barrier distributions and fusion barrier distributions for ^{40}Ca+^{46,48,50}Ti.

$D_{\mathrm{qel}}(E)$ obtained from Eq. (4) is shown in Fig. 9 and $D_{\mathrm{el}}(E)$ using Eq. (5) can be seen in Fig. 10, together with the fusion results. The fusion radii used to scale down D_{fus} are those obtained in Sec. II A. It should be remembered that the $D_{\mathrm{qel,el}}$ values are more precise than the D_{fus} ones for two basic reasons: (a) They involve a first derivative, and (b) the experiment is far easier to perform and therefore a higher precision can be achieved.

The agreement between the two sets of data in Fig. 9 is remarkably good; the shapes are quite well reproduced but the fusion data give slightly narrower and more strongly peaked barrier distributions than the quasielastic. Similar results were obtained in Ref. [11].

The elastic barrier distributions in Fig. 10 are shorter and broader than the fusion ones. This disagreement cannot be due to normalization problems in the definitions of the elastic barrier distributions since the shapes do not look alike. Again, similar results were found by the Canberra group [12], when supposedly only elastic scattering data were used.

It is then concluded that $D_{\mathrm{qel}}(E)$ given by Eq. (4) strongly resembles $D_{\mathrm{fus}}(E)$ and therefore seems to be the

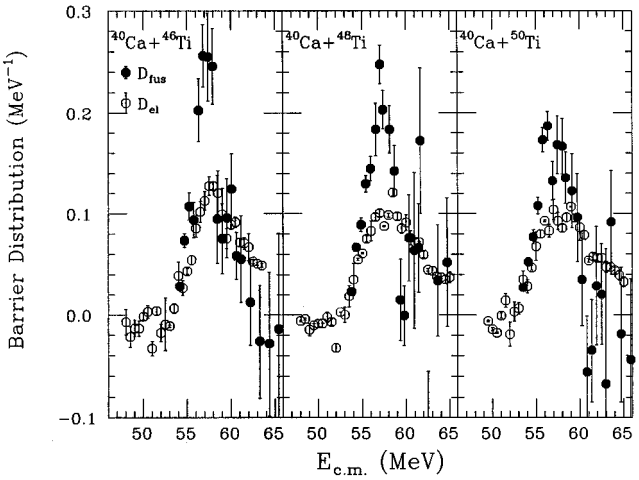

FIG. 10. Comparison between elastic barrier distributions and fusion barrier distributions for ^{40}Ca+^{46,48,50}Ti.

TABLE II. Surface vibration coupling parameters for Ca and Ti nuclei.

Nucleus	β_2	E_{2^+} (MeV)	β_3	E_{3^-} (MeV)
^{50}Ti	0.166	1.555	0.156	4.410
^{48}Ti	0.269	0.983	0.147	3.358
^{46}Ti	0.317	0.889	0.122	3.059
^{40}Ca	0.122	3.904	0.330	3.736

TABLE III. Neutron transfer Q values (MeV) for the $1n$, $2n$, $3n$, and $4n$ projectile pickup reactions for ^{40}Ca+^{46,48,50}Ti.

System	Q_{1n}	Q_{2n}	Q_{3n}	Q_{4n}
^{40}Ca + ^{50}Ti	−2.6	0.8	−2.9	−0.7
^{40}Ca+^{48}Ti	−3.3	−0.7	−5.9	−4.3
^{40}Ca+^{46}Ti	−4.8	−2.9	−11.2	−12.4

most suitable representation for unresolved elastic plus quasielastic data. The first work to report this kind of research [11] was done for very asymmetric systems. Recently, the technique has been successfully used for more symmetric systems [18]. We have tested the technique for very symmetric systems and obtained very satisfactory results. One concludes that this could be a very important tool in fusion research. As mentioned before, the experiments to be carried out, though challenging, are not as difficult as the fusion ones. An immediate application could appear when investigating the fusion properties of unstable nuclei. Because of the low beam currents, a fusion experiment might not be practical. However, exploratory elastic-quasielastic runs could be performed to see if these barrier distributions show special features that would make it worth spending a large amount of time on a full scale fusion experiment.

D. Coupled-channel calculations

Simplified coupled-channel calculations similar to those produced by the code CCMOD [19,20] can be performed to account quantitatively for the contributions of SVC's and TC's. Briefly, under a number of approximations, it can be shown that the result of coupling to a number N of phonon-transfer channels is to split the original uncoupled barrier in $N+1$ different barriers. Then, the fusion cross section can be expressed as

$$\sigma_{\rm fus}(E)=\sum_{\alpha=1}^{N+1} w_\alpha \sigma_\alpha(E,V_b+\lambda_\alpha), \tag{7}$$

where V_b is the uncoupled barrier, λ_α are the eigenvalues of the coupling matrix, and the weight factors w_α are directly related to its eigenvectors [20]. The off-diagonal phonon coupling elements involve complicated integrals and only linear terms in β_λ will be considered [21]. In this model, there is no reliable *a priori* estimate for the magnitude of the off-diagonal transfer coupling terms. They will eventually be varied to match the data. Transfers to excited states, which all have negative Q values, are not considered. In addition, the positions and curvatures of the new barriers are obtained by finding the maxima of $V_b(r)+\lambda_\alpha(r)$.

The coupling parameters used for the Ca+Ti systems are listed in Tables II and III and were obtained from Refs. [22–24]. The Christensen-Winther parametrization of the nuclear potential was used; however, its strength was adjusted to match the data.

The most basic calculation is the uncoupled one. Calculations involving couplings will mostly differ from the uncoupled one in the near-barrier region ($\sigma_{\rm fus}\leqslant 150$ mb). For higher energies, coupling effects are not very important and therefore the coupled and uncoupled solutions give similar results. Once the nuclear potential strength is adjusted to match the high energy part of the data, SVC's can be incorporated. Those considered here are one-phonon couplings to the lowest 2^+ and 3^- states of both target and projectile. Both coupled and uncoupled calculations can be seen in Fig. 11. Clearly, the measured fusion cross sections for ^{40}Ca $+^{46}$Ti are well reproduced. The low energy cross sections for ^{40}Ca+^{48}Ti are underestimated slightly, and those for ^{40}Ca+^{50}Ti are grossly underestimated if only SVC's are included.

The next step is to include transfer couplings. Here we make use of the benefit of choosing systems for which SVC's and TC's have the opposite target-mass dependence; i.e., target SVC's have to be more important for ^{46}Ti than for ^{50}Ti. However, by invoking SVC's the cross sections for ^{46}Ti can be reproduced but not the ^{50}Ti ones; therefore, the excess in cross section for the latter target should not originate from SVC's but rather from TC's. As mentioned before, the issue of how TC's affect the subbarrier fusion cross sections is not completely understood. There is clear evidence indicating that neutron-transfer reactions play a very important role [7,10], particularly those with positive Q values. Our way of dealing with this subject was to couple to the neutron-transfer channel with the most positive Q value, which in this case corresponds to the projectile pickup of two neutrons. The transfer strengths were varied to produce a

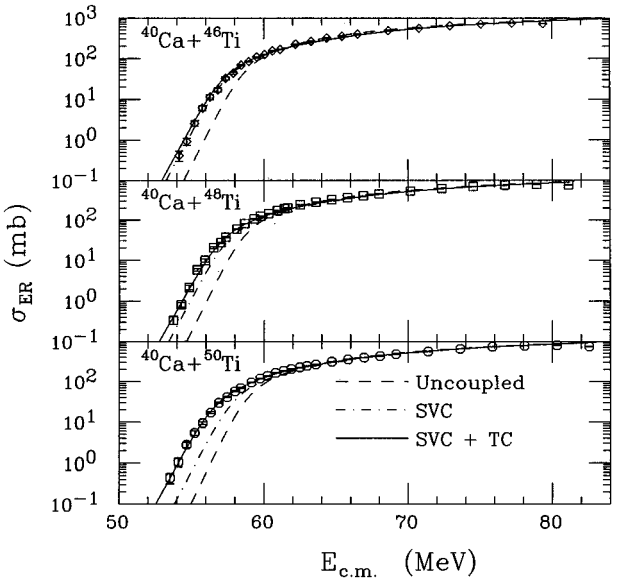

FIG. 11. Fusion excitation functions for ^{40}Ca+^{46,48,50}Ti. The dashed curve is from a no-coupling calculation, and the dot-dashed and solid lines show the results of coupled-channel calculations.

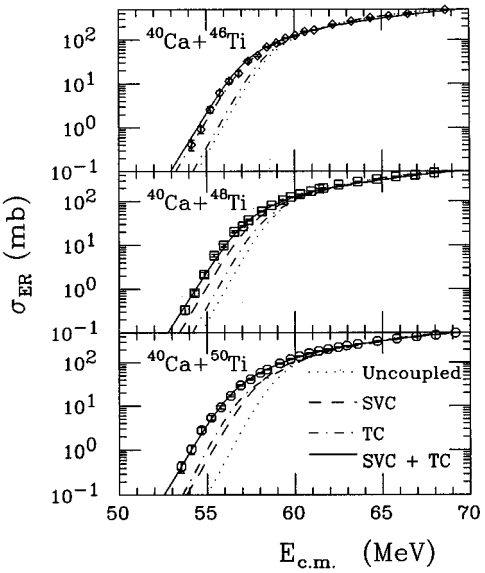

FIG. 12. Illustration of the individual contributions of the surface vibration channels and of the transfer channel to the fusion excitation functions for ^{40}Ca+^{46,48,50}Ti at near-barrier energies.

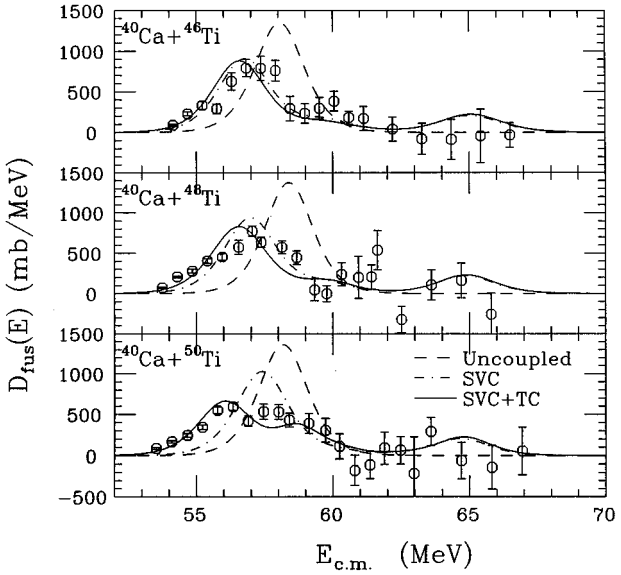

FIG. 13. Comparison of the experimental fusion barrier distributions for ^{40}Ca+^{46,48,50} to the results of coupled-channel calculations.

satisfactory match between calculated and measured fusion cross sections. The results can be seen in Fig. 11. The transfer strengths (the F values in Ref. [20]) that best fit the data were equal to 1.5 MeV for ^{40}Ca+^{50}Ti and 1.0 MeV for ^{40}Ca+^{48}Ti. Since phonon couplings give a good account of the ^{40}Ca+^{46}Ti excitation function, obtaining an optimum value of the transfer strength for this system is not meaningful. For comparison purposes, a strength of 1.0 MeV was used for this latter system, resulting in little deviation from the SVC calculations, due to the negative nature of the $2n$ pickup channel Q value (-2.9 MeV). To make apparent the individual contributions of SVC's and TC's to the fusion cross section, the calculated fusion excitation functions are plotted on an expanded energy scale in Fig. 12. Although we have demonstrated in a model-independent way that TC's dominate over SVC's for ^{40}Ca+^{50}Ti, these coupled-channel calculations indicate that for the other two systems, SVC's are mainly responsible for the subbarrier fusion enhancement.

The barrier distributions from these calculations are compared with the experimental results in Fig. 13. Because of the difficulties in extracting fusion barrier distributions, it is not our intention to use this figure to demonstrate the presence and effect of TC's. However, it can be seen that the agreement between data and model calculations is good. The observation that the peak in the experimental fusion and quasielastic barrier distributions get shorter and wider as one moves from ^{46}Ti to ^{50}Ti is reproduced in the simplified coupled-channel calculations as a result of the transfer couplings. The positions of the individual barriers resulting from the couplings are also of interest. These barrier positions and their corresponding weight factors w_α in Eq. (7), are displayed in Fig. 14.

E. Deduction of the $\langle \ell \rangle(E)$

Finally, we would like to mention one other quantity that can be derived from the fusion excitation function with certain assumptions. Sahm *et al.* [25] first suggested that one could deduce the mean value of the ℓ distribution $\langle \ell \rangle$ at a given energy E from the dependence of the fusion cross section at energies less than E. This problem has been explored more recently by Balantekin *et al.* [26]. The starting point of the model is the following expression:

$$\sigma_{\rm fus}(E)=\sum_{\ell=0}^{\infty}\frac{\pi\hbar^2}{2\mu E}(2\ell+1)T_\ell(E). \tag{8}$$

The key hypothesis is that R_b is independent of ℓ so that one can write

$$T_\ell(E)=T_0\left(E-\frac{\hbar^2\ell(\ell+1)}{2\mu R_b^2(E)}\right). \tag{9}$$

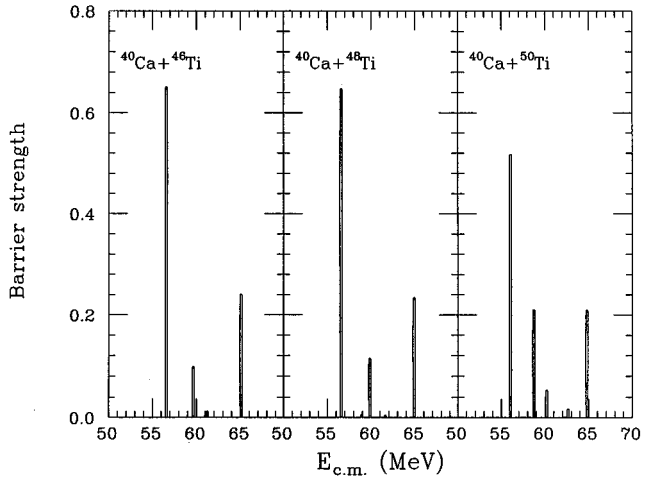

FIG. 14. Barrier strengths (w_α) for the different barriers resulting from the coupled-channel calculations that includes SVC's and TC's.

For spherical targets and projectiles it is safe to assume that $R_b^2(E)=R_b^2$. An expression for the first moment can be obtained after a change of variables:

$$\langle \ell \rangle(E)=\frac{\mu R_b^2}{\hbar^2 E\sigma_{\rm fus}(E)}\int_0^E dE' E'\sigma(E') \times\left[\frac{2\mu R_b^2}{\hbar^2}(E-E')+\frac{1}{4}\right]^{-1/2}. \quad (10)$$

Clearly this model relies on the validity of Eq. (8). However, recent experimental studies indicate the presence of a set of barriers rather than a single one. Under these conditions, the fusion cross section is written as

$$\sigma_{\rm fus}(E)=\sum_\alpha w_\alpha \sigma_{\rm fus}(E,V_{b\alpha},R_{b\alpha},\hbar\omega_\alpha) \quad (11)$$

or

$$\sigma_{\rm fus}(E)=\sum_\alpha w_\alpha \sum_\ell \frac{\pi\hbar^2}{2\mu E}(2\ell+1)T_{\ell\alpha}(E), \quad (12)$$

an effective transmission coefficient can be defined as

$$T_\ell^{\rm eff}(E)=\sum_\alpha w_\alpha T_{\ell\alpha}(E), \quad (13)$$

and it will be very difficult to express $T_\ell^{\rm eff}(E)$ as in Eq. (9). We have tested the possibilities of this method by using the result of a coupled-channel calculation as an input to Eq. (10). We have concluded that the method works quite well, even for strong couplings.

Clearly, the extraction of $\langle \ell \rangle$ values involves several assumptions and therefore these values should be considered an estimate of the compound nucleus mean angular momentum, rather than a measurement of it. However, in the absence of the latter, these estimates can be useful when, for instance, performing statistical model calculations.

The extraction of $\langle \ell \rangle$ values for the systems under study is of interest because a previous study of ^{32}S+^{100}Mo and ^{36}S+^{96}Mo [27] showed that a result of transfer channel coupling is to make the compound nucleus spin distribution broader. Our results can be seen in Fig. 15, where the open symbols come from using Eq. (10) and the solid line is the result of the coupled-channel calculation that gives a good account of the fusion cross section, while the dotted line comes from the uncoupled one. It is reassuring to observe that the results in Fig. 15 indicate a broader spin distribution for ^{50}Ti than for ^{46}Ti. The agreement between the coupled-channel calculations and the values derived from the fusion excitation function using Eq. (10) is to be expected since the centrifugal potential in the coupled-channel calculations is treated in a similar way to Eq. (9) for each individual barrier.

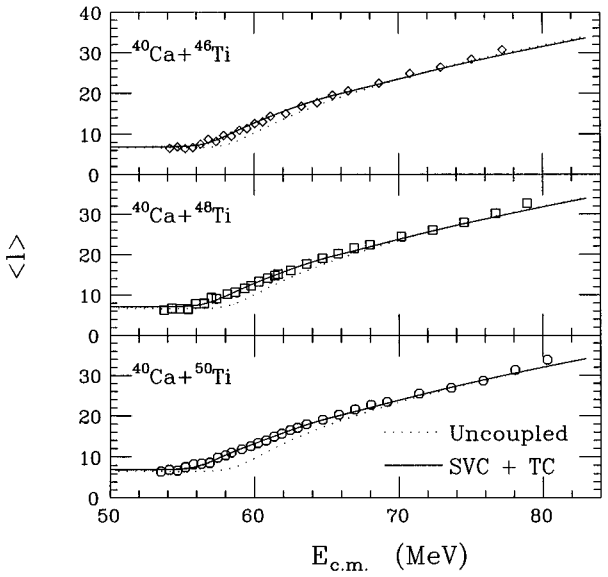

FIG. 15. Mean compound nucleus angular momentum as extracted from the experimental fusion excitation functions using Eq. (10) (open symbols) and as given by coupled-channel calculations (solid curves) as a function of the center-of-mass energy.

IV. CONCLUSIONS AND OUTLOOK

In summary, experiments to measure the fusion excitation functions as well as quasielastic angular distributions and excitation functions were performed for the systems ^{40}Ca + ^{46,48,50}Ti at energies close to the Coulomb barrier. Our target and projectile selection has enabled us to highlight the relative effect of neutron-transfer reactions and surface vibration couplings on the magnitude of the near-barrier fusion cross sections. A comparative analysis of the fusion excitation functions for the three systems shows that ^{50}Ti has the largest subbarrier enhancement while ^{46}Ti has the smallest. Because of the isotopic dependence of the collectivities and transfer Q values, this can only happen under the presence of strong transfer couplings. The effects of surface vibration couplings alone would give the opposite result. This interpretation is additionally supported by the fact that the ^{50}Ti target also exhibits the broadest barrier distribution.

We have obtained barrier distributions from both fusion and quasielastic excitation functions, this being the first time that such comparisons have been published for very symmetric systems. The similarity between these barrier distributions is remarkable.

Coupled-channel calculations were performed assuming first order surface vibration coupling terms and constant neutron-transfer couplings. The former included coupling to the lowest 2^+ and 3^- of both target and projectile. The transfer coupling strengths were varied to match the fusion excitation function, with similar values being obtained for all three systems. The differing effects of the transfer couplings are explained by the change of neutron-transfer Q values as the mass of the target varies. Despite the simplicity of these calculations, we were able to reproduce the experimental results.

The results of this work, together to those from [7,16,10], clearly point out the importance of coupling to transfer channels with positive Q values. We would like to suggest two additional experiments that we think are of interest. The first proposed experiment would be to measure the fusion excitation functions for ^{40}Ca+^{208}Pb. Both target and projectile have double closed shells, but the neutron richness of ^{208}Pb together with the relative neutron deficiency of ^{40}Ca gives

rise to very positive Q values. In addition, recent measurements were reported for $^{40}Ca+^{192}Os$ and ^{194}Pt [3], and an interesting comparison could be made between deformed Os, Pt, and spherical ^{208}Pb.

To motivate the projectile and target selection for the second proposed experiment, let us first assume that under the right circumstance—positive Q values—a flow of neutrons can effectively take place and enhance the fusion cross section. One realizes then that all the studies done so far involved a flow of neutrons from the heavier partner to the lighter one, and the system evolves to a more symmetric shape before fusioning. It can be argued that if the flow of neutrons goes in the opposite direction, i.e., from lighter partner to heavier one, fusion would be further helped since the system would evolve toward a more asymmetric entrance channel configuration. In other words, assuming that the lighter partner is the projectile, only projectile neutron pickup has been investigated. Perhaps target pickup has an even stronger influence. Unfortunately, there are not many target-projectile combinations that can be used. The most promising one seems to be $^{48}Ca+^{58}Ni$.

This work was supported by the U.S. Department of Energy.

[1] M. Beckerman, Phys. Rep. **129**, 145 (1985).
[2] J. R. Leigh, M. Dasgupta, D. J. Hinde, J. C. Mein, C. R. Morton, R. C. Lemmon, J. P. Lestone, J. O. Newton, H. Timmers, and J. X. Wei, Phys. Rev. C **52**, 3151 (1995).
[3] J. D. Bierman, P. Chan, J. F. Liang, M. P. Kelly, A. A. Sonzogni, and R. Vandenbosch, Phys. Rev. Lett. **76**, 1587 (1996).
[4] A. M. Stefanini, D. Ackerman, L. Corradi, D. R. Napoli, C. Petrache, P. Spolaore, P. Bednarczyk, H. Q. Zhang, S. Beghini, G. Montagnoli, L. Mueller, F. Scarlassara, G. F. Segato, F. Somarel, and N. Rowley, Phys. Rev. Lett. **74**, 864 (1995).
[5] W. Henning, F. L. H. Wolfs, J. P. Schiffer, and K. E. Rehm, Phys. Rev. Lett. **58**, 318 (1987).
[6] P. H. Stelson, H. J. Kim, M. Beckerman, D. Shapira, and R. L. Robinson, Phys. Rev. C **41**, 1584 (1990).
[7] A. M. Stefanini, D. Ackerman, L. Corradi, J. H. He, G. Montagnoli, S. Beghini, F. Scarlassara, and G. F. Segato, Phys. Rev. C **52**, R1727 (1995).
[8] R. G. Stokstad, Y. Eisen, S. Kaplanis, D. Pelte, U. Smilansky, and I. Tserruya, Phys. Rev. C **21**, 2427 (1980).
[9] D. E. Di Gregorio, J. O. Fernandez Niello, A. J. Pacheco, D. Abriola, S. Gil, A. O. Macchiavelli, J. E. Testoni, P. R. Pascholati, V. R. Vanin, R. Liguori Neto, N. Carlin Filho, M. M. Coimbra, P. R. Silveira Gomes, and R. G. Stokstad, Phys. Lett. B **176**, 322 (1986).
[10] H. Timmers, D. Ackerman, L. Corradi, J. H. He, A. M. Stefanini, G. Montagnoli, S. Beghini, F. Scarlassara, G. F. Segato, and N. Rowley, Instituto Nazionale di Fisica Nucleare, Laboratori Nazionali di Legnaro, Annual Report 1995, p. 88.
[11] H. Timmers, J. R. Leigh, M. Dasgupta, D. J. Hinde, R. C. Lemmon, J. C. Mein, C. R. Morton, J. O. Newton, and N. Rowley, Nucl. Phys. **A584**, 190 (1995).
[12] N. Rowley, H. Timmers, J. R. Leigh, M. Dasgupta, D. J. Hinde, J. C. Mein, C. R. Morton, and J. O. Newton, Phys. Lett. B **373**, 23 (1996).
[13] J. X. Wei, J. R. Leigh, D. J. Hinde, J. O. Newton, R. C. Lemmon, S. Elfstrom, and J. X. Chen, Phys. Rev. Lett. **67**, 3368 (1991).
[14] K. E. Rehm, F. L. Wolf, A. M. van den Berg, and W. Henning, Phys. Rev. Lett. **55**, 280 (1985).
[15] A. M. Stefanini, J. Xu, L. Corradi, G. Montagnoli, H. Moreno, Y. Nagashima, L. Mueller, M. Narayanasamy, D. R. Napoli, P. Spolaore, S. Beghini, F. Scarlassara, G. F. Segato, F. Soramel, C. Signorini, H. Esbensen, S. Landowne, and G. Pollarolo, Phys. Lett. B **240**, 306 (1990).
[16] H. A. Aljuwair, R. J. Ledoux, M. Beckerman, S. B. Gazes, J. Wiggins, E. R. Cosman, R. R. Betts, S. Saini, and O. Hansen, Phys. Rev. C **30**, 1223 (1984).
[17] N. Rowley, G. R. Satchler, and P. H. Stelson, Phys. Lett. B **254**, 25 (1991).
[18] H. Timmers, D. Ackerman, L. Corradi, J. H. He, A. M. Stefanini, G. Montagnoli, S. Beghini, F. Scarlassara, and G. F. Segato, Instituto Nazionale di Fisica Nucleare, Laboratori Nazionali di Legnaro, Annual Report 1995, p. 90.
[19] M. Dasgupta, A. Navin, Y. K. Agarwal, C. V. K. Baba, H. C. Jain, M. L. Jhingan, and A. Roy, Nucl. Phys. **A539**, 351 (1992).
[20] C. H. Dasso and S. Landowne, Comput. Phys. Commun. **46**, 187 (1987).
[21] K. Hagino, N. Takigawa, M. Dasgupta, D. J. Hinde, and J. R. Leigh, Phys. Rev. C **55**, 276 (1997).
[22] S. Raman, C. H. Malarkey, W. T. Milner, C. W. Nestor, Jr., and P. H. Stelson, At. Data Nucl. Data Tables **36**, 1 (1987).
[23] R. H. Spear, At. Data Nucl. Data Tables **42**, 55 (1989).
[24] M. Fujiwara, Y. Fujita, S. Imanishi, S. Morinobu, T. Yamazaki, H. Ikegami, K. Katori, and S. I. Haykawa, Phys. Rev. C **32**, 830 (1985); M. Fujiwara, S. Morinobu, M. Tosaki, H. Ito, I. Katayama, H. Ikegami, S. I. Hayakawa, N. Ikeda, H. Ohsumi, A. Higashi, and K. Katori, *ibid.* **35**, 1257 (1987); A. Higashi, K. Katori, M. Fujiwara, H. Ikegami, I. Katayama, S. Morinobu, M. Tosaki, S. I. Hayakawa, N. Ikeda, and H. Miyatake, *ibid.* **39**, 1286 (1989).
[25] C. C. Sahm, H.-G. Clerc, K.-H. Schmidt, W. Reisdorf, P. Armbruster, F. P. Hessberger, J. G. Keller, G. Münzenberg, and D. Vermeulen, Nucl. Phys. **A441**, 316 (1985).
[26] A. B. Balantekin, J. DeWeerd, and S. Kuyucak, Phys. Rev. C **54**, 1853 (1996).
[27] H.-J. Hennrich, G. Breitbach, W. Kuhn, V. Metag, R. Novotny, D. Habs, and D. Schwalm, Phys. Lett. B **258**, 275 (1991).